

Article

## Combustion Synthesis and Photoluminescence Properties of Red-Emitting $\text{CaAlSiN}_3:\text{Eu}^{2+}$ Phosphor for White-LEDs

Shyan-Lung Chung <sup>1,2,\*</sup> and Shu-Chi Huang <sup>1</sup>

<sup>1</sup> Department of Chemical Engineering, National Cheng Kung University, Tainan 70101, Taiwan; E-Mail: n38981266@mail.ncku.edu.tw

<sup>2</sup> Advanced Optoelectronic Technology Center, National Cheng Kung University, Tainan 70101, Taiwan

\* Author to whom correspondence should be addressed; E-Mail: slchung@mail.ncku.edu.tw; Tel.: +886-6275-7575 (ext. 62654); Fax: +886-6234-4496.

External Editor: Wen-Hsiang Hsieh

Received: 18 October 2014; in revised form: 19 November 2014 / Accepted: 27 November 2014 /

Published: 5 December 2014

---

**Abstract:** A combustion synthesis method has been developed for synthesis of  $\text{Eu}^{2+}$  doped  $\text{CaAlSiN}_3$  phosphor and its photoluminescence properties were investigated. Ca, Al, Si, and  $\text{Eu}_2\text{O}_3$  powders were used as the Ca, Al, Si and Eu sources. The addition of  $\text{NaN}_3$ ,  $\text{NH}_4\text{Cl}$  and  $\text{Si}_3\text{N}_4$  powders was found to increase significantly the product yield. These powders were mixed and pressed into a compact, which was then wrapped up with an igniting agent (*i.e.*,  $\text{Mg}+\text{Fe}_3\text{O}_4$ ). The compact was ignited by electrical heating under a  $\text{N}_2$  pressure of  $\leq 1.0$  MPa. Effects of these experimental parameters on the product yield were investigated and a reaction mechanism was proposed. The synthesized  $\text{CaAlSiN}_3:\text{Eu}^{2+}$  phosphor absorbs light in the region of 200–600 nm and shows a broad band emission in the region of 500–800 nm due to the  $4f^65d^1 \rightarrow 4f^7$  transition of  $\text{Eu}^{2+}$ . The sample doped with  $\text{Eu}^{2+}$  at the optimized molar ratio of 0.04 is efficiently excited by the blue light (460 nm) and generates emission peaking at ~650 nm with peak emission intensity ~106% of a commercially available phosphor,  $\text{YAG}:\text{Ce}^{3+}$  (P46-Y3). The internal quantum efficiency of the synthesized phosphor was measured to be 71%, compared to 69% of the  $\text{YAG}:\text{Ce}^{3+}$  (P46-Y3).

**Keywords:**  $\text{CaAlSiN}_3:\text{Eu}^{2+}$ ; nitridosilicate phosphor; LED lighting; combustion synthesis

---

## 1. Introduction

White light LED lighting has been replacing conventional lighting and becoming the next generation lighting device due to advantages such as energy efficiency, long lifetime, compactness, environmental friendliness and designable features [1–4]. Phosphors are essential materials for the fabrication of the LED lighting devices and their properties significantly affect the performance of the devices. Among various types of phosphor, the type with red emission has been considered to be the most urgent one to be developed for two main reasons: Its use can improve the color rendering of the currently commercialized LED lighting devices and conventional red phosphors (e.g.,  $\text{Sr}_{1-x}\text{Ca}_x\text{S}:\text{Eu}^{2+}$  and  $\text{Y}_2\text{O}_2\text{S}:\text{Eu}^{3+}$ ) suffer from poor chemical stability and low quantum efficiency. In the past decade, a class of phosphors (*i.e.*, rare-earth doped nitridosilicates) were discovered and shown to be ideal for application in LED lighting due to their superior properties such as high quantum efficiency, long wavelength (red) emission and high thermal and chemical stability [5]. Two major types of nitridosilicate have been developed as the host lattices for the nitridosilicate phosphors, namely alkaline-earth silicon nitrides ( $\text{M}_2\text{Si}_5\text{N}_8$ ,  $\text{M} = \text{Ca}, \text{Sr}$  and  $\text{Ba}$ , often referred to as 2-5-8 phosphors) and alkaline-earth aluminum silicon nitrides ( $\text{MAlSiN}_3$ ,  $\text{M} = \text{Mg}, \text{Ca}$  and  $\text{Sr}$ , often referred to as 1-1-1-3 phosphors). Many methods have been developed for the synthesis of nitridosilicate phosphors including [5] solid state reaction (SSR) [6], carbothermal reduction and nitridation (CRN) [7], gas pressure sintering [8], reaction between metals and silicon diimide [9], gas reduction and nitridation [10], high pressure ammonothermal method [11], spark plasma sintering [12], alloy-nitridation [13], nitrate reduction [14] and combustion synthesis (SHS) [15]. However, many of these methods utilize costly and oxygen- or moisture-sensitive chemicals as the starting materials, and most of the methods are carried out under severe synthesis conditions (e.g., high temperatures, high pressures and long reaction time). These problems may hinder the practical application of the methods. Further studies in the development of the synthesis method are thus needed so that the nitridosilicate phosphors can be produced under easier synthesis conditions with low production costs, thus boosting the practical applications of LED lighting.

In our previous study [16], a combustion synthesis method was developed for the synthesis of  $\text{Eu}^{2+}$ -doped  $\text{Ca}_2\text{Si}_5\text{N}_8$  phosphor:  $\text{Ca}$ ,  $\text{Si}$  and  $\text{Eu}_2\text{O}_3$  powders were used as the  $\text{Ca}$ ,  $\text{Si}$  and  $\text{Eu}$  sources and  $\text{NaN}_3$ ,  $\text{NH}_4\text{Cl}$  and  $\text{Si}_3\text{N}_4$  were added to enhance the product yield. The synthesis reaction was triggered by the combustion of an igniting agent, which wrapped up the reactant compact. A product yield of  $\sim 71\%$  was obtained under a  $\text{N}_2$  pressure of 0.7 MPa. In addition to easy handling of the reactants and a low  $\text{N}_2$  pressure required ( $\sim 0.7$  MPa), the method developed possesses many other advantages including simple and inexpensive equipment required, relatively low cost of the reactants, a fast reaction and short processing time, potential capability for mass production and possibly low production costs.

When comparing with 2-5-8 phosphors, 1-1-1-3 phosphors were found to have many superior properties [17–19] such as an even higher thermal stability, a longer emission wavelength and a higher quantum efficiency. However, the 1-1-1-3 phosphors were also found to require even more severe conditions for their synthesis (as compared to that of the 2-5-8 phosphors) [20]. In the present study, the combustion synthesis method developed in our previous study [16] was tested and modified for the synthesis of  $\text{CaAlSiN}_3:\text{Eu}^{2+}$  phosphor. Reactants were chosen to be those which could be handled in ambient air and the process was designed to be carried out under a low  $\text{N}_2$  pressure limited to our SHS reactor ( $\leq 1.0$  MPa). The development of the process and the effects of process parameters on the product

yield will be described and a reaction mechanism will be proposed. The luminescent properties of the synthesized phosphor will also be reported and discussed.

## 2. Results and Discussion

### 2.1. Optimum Synthesis Condition and Combustion Phenomena

After a series of experiments (some of which will be described later), an optimum synthesis condition (achieving the highest product yield) was found to be that the reactant compact had a composition of  $\text{Ca:Al:Si:NaN}_3\text{:NH}_4\text{Cl:Si}_3\text{N}_4\text{:Eu}_2\text{O}_3 = 1-2x:1:0.25:3.5:0.6:0.25:x$  and that the combustion synthesis reaction was carried out under a  $\text{N}_2$  pressure of 0.9 MPa (all the reactant compositions were expressed as molar ratios in this work). Under such an optimum synthesis condition, it was observed that the igniting agent was ignited when the heating power had been turned on for  $\sim 10$  s and subsequently, the combustion wave propagated down the compact. During propagation of the combustion wave, visible radiation was observed to be emitted from the interior indicating the occurrence of the synthesis reaction of the reactant compact (this visible radiation was observed to last for  $\sim 5$  s). Figure 1 shows typical temperature-time histories measured by thermocouples A and B. Both profiles show abrupt increases in temperature, which were caused by heat transfer from the combustion waves (when approaching the points of measurement) and also by the onset of their own combustion. The abrupt increase in profile (b) occurred several seconds after that of profile (a), indicating that the combustion of the reactant compact was caused by heating by the combustion of the igniting agent. The maximum combustion temperatures of the igniting agent and the reactant compact were measured to be  $\sim 2230$  °C and  $\sim 1730$  °C, respectively.

**Figure 1.** Typical temperature-time histories during combustion reaction.

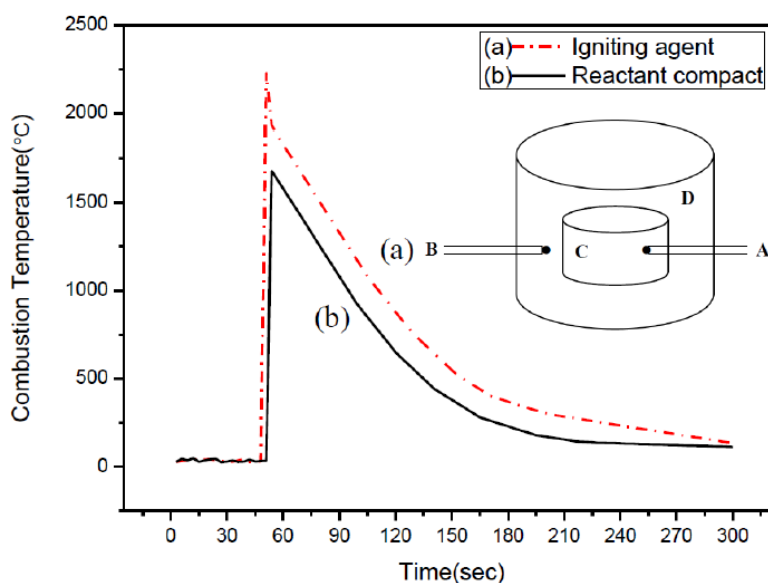


Figure 2 is a photograph of the as-synthesized product obtained under the optimum synthesis condition (*i.e.*,  $\text{Ca:Al:Si:NaN}_3\text{:NH}_4\text{Cl:Si}_3\text{N}_4\text{:Eu}_2\text{O}_3 = 0.92:1:0.25:3.5:0.6:0.25:0.04$  under a  $\text{N}_2$  pressure of 0.9 MPa). As can be seen, the as-synthesized product was highly porous. The outer layer (black in color) is the combustion product of the igniting agent and the inside portion (red in color) is the synthesized

phosphor. After removing the outer layer, the product was ground by using a mortar and pestle for ~3 min to powder for characterization.

**Figure 2.** A photograph of the as-synthesized product obtained under the optimum synthesis condition. The outer layer (black in color) is the combustion product of the igniting agent and the inside portion (red in color) is the synthesized phosphor.

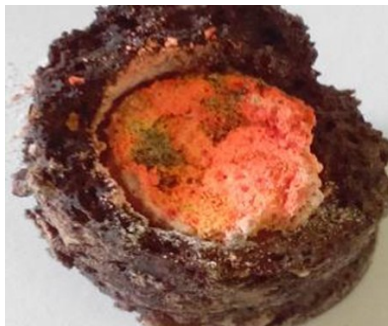
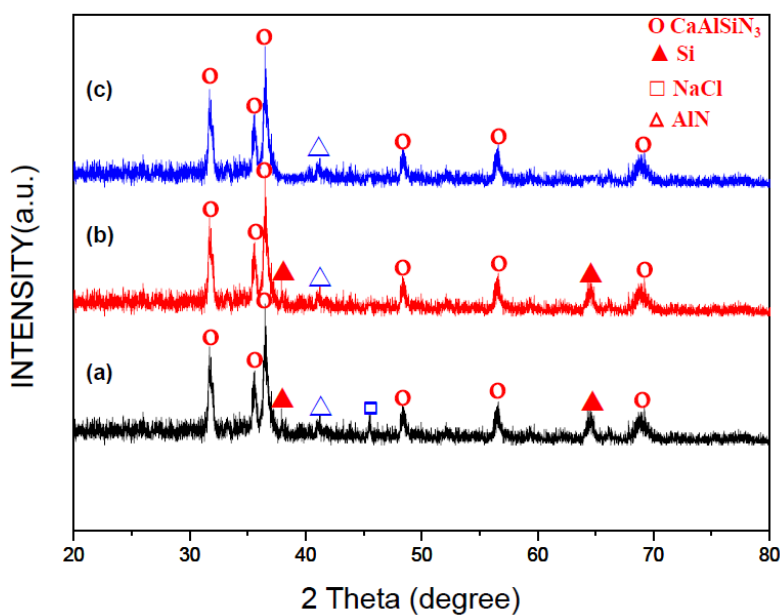


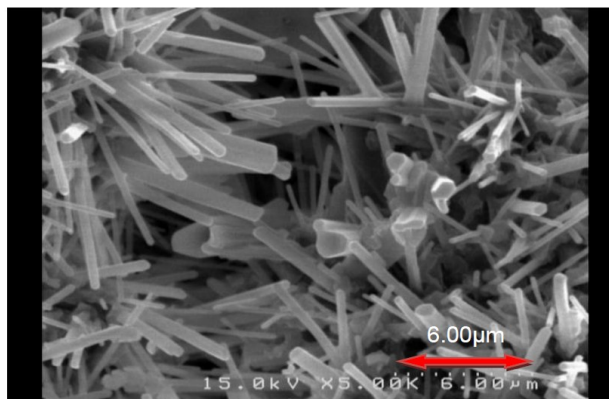
Figure 3a is an XRD pattern of the as-synthesized product obtained under the optimum synthesis condition. As can be seen, in addition to the phase of  $\text{CaAlSiN}_3:\text{Eu}^{2+}$  (JCPDS No.39-0747), AlN (JCPDS No. 88-2363), NaCl (JCPDS No. 88-2300) and residual Si (JCPDS No. 79-0613) were also detected. As mentioned previously [16], NaCl could be removed by washing the product with water and residual Si could be removed by washing the product with an acid. Figure 3b,c are the XRD patterns of the products after these washings.

**Figure 3.** XRD patterns of the products: (a) as-synthesized; (b) after washing with water; and (c) after washing with water and an acid.



The powder thus obtained (after removing NaCl and the residual Si) appeared red in color and most of the particles were observed (see Figure 4) to be columnar in shape (with a diameter ranging from 0.1 to 0.8  $\mu\text{m}$  and a length ranging from 5 to 10  $\mu\text{m}$ ). The average particle size ( $d_{50}$ ) was measured by the particle size analyzer to be 8.8 $\mu\text{m}$

**Figure 4.** A typical SEM photograph of the product (Ca:Al:Si:NaN<sub>3</sub>:NH<sub>4</sub>Cl:Si<sub>3</sub>N<sub>4</sub>:Eu<sub>2</sub>O<sub>3</sub> = 0.92:1:0.25:3.5:0.6:0.25:0.04) after grinding and removing NaCl and the residual Si.



## 2.2. Effects of Process Parameters on Product Yield

### 2.2.1. Effects of NH<sub>4</sub>Cl and NaN<sub>3</sub>

Figure 5 shows the effects of NaN<sub>3</sub> and NH<sub>4</sub>Cl contents on the product yield. The contents of other reactants and the N<sub>2</sub> pressure were kept the same as the optimum synthesis condition. As can be seen, the product yield was very low (5% or 10%, respectively) when no NaN<sub>3</sub> or NH<sub>4</sub>Cl was added. The product yield increases with increasing NH<sub>4</sub>Cl content to a maximum of ~71% (at a molar ratio of 0.6) and begins to decrease with further increase in NH<sub>4</sub>Cl content. In the case of adding NaN<sub>3</sub>, the product yield is seen in Figure 5 (curve (a)) to increase with increasing NaN<sub>3</sub> content to ~74% (at a molar ratio of 3.5) and becomes relatively unaffected with further increase in the NaN<sub>3</sub> content. In our previous studies on the combustion synthesis of Si<sub>3</sub>N<sub>4</sub> [21], NH<sub>4</sub>X (X = F, Cl, Br or I with NH<sub>4</sub>Cl being the most effective) and NaN<sub>3</sub> were found necessary for the formation of Si<sub>3</sub>N<sub>4</sub> and a reaction mechanism was proposed: Si was considered to react with HX (produced by thermal decomposition of NH<sub>4</sub>X), converting itself to more reactive species, SiX<sub>x</sub>. SiX<sub>x</sub> was then reduced by Na vapor (produced by thermal decomposition of NaN<sub>3</sub>) and subsequently, nitridation of Si takes place, resulting in the formation of Si<sub>3</sub>N<sub>4</sub>. NH<sub>4</sub>X and NaN<sub>3</sub> were thus referred to as catalytic and reducing agents, respectively. In the present study, the formation of CaAlSiN<sub>3</sub>:Eu<sup>2+</sup> is believed to follow a similar mechanism. Both NH<sub>4</sub>Cl and NaN<sub>3</sub> are thus required to achieve high products.

In the present study, Ca, Al were also considered to react with HCl forming CaCl<sub>2</sub> and AlCl<sub>3</sub>. As illustrated in Figure 6, SiCl<sub>x</sub>, CaCl<sub>2</sub>, and AlCl<sub>3</sub> were then reduced by Na vapor and subsequently, nitridation of the reduced species takes place, forming the host lattice. In the meantime, Eu<sub>2</sub>O<sub>3</sub> may be reduced by Na vapor or H<sub>2</sub> (generated by reactions of Si and HCl, see Figure 6) and incorporates into the host lattice forming the product phase, CaAlSiN<sub>3</sub>:Eu<sup>2+</sup>.

When the NH<sub>4</sub>Cl content is low (at a molar ratio of <0.6), increasing the NH<sub>4</sub>Cl content (while keeping the contents of other reactants constant) increases the concentration of HCl, promoting the formation of the chlorides of Si, Ca, and Al. Formation of CaAlSiN<sub>3</sub>:Eu<sup>2+</sup> is therefore enhanced, resulting in a higher product yield. When the NH<sub>4</sub>Cl content was higher than a molar ratio of 0.6, a violent gas evolution occurred during the combustion. Much powder was thus thrown out of the reactant compact and deposited on the reactor walls. (This powder was collected and identified by XRD analysis to be

mostly  $\text{CaAlSiN}_3:\text{Eu}^{2+}$ ). The product yield thus decreases with increasing  $\text{NH}_4\text{Cl}$  content. When increasing the  $\text{NaN}_3$  content, the concentration of Na vapor is increased, promoting the reduction and thus the nitridation reactions. The product yield thus increases with increasing  $\text{NaN}_3$  content. As the  $\text{NaN}_3$  content is further increased (with a molar ratio  $>3.5$ ), the product yield is relatively unaffected because a sufficient concentration of Na has been generated.

Figure 5. Effects of (a)  $\text{NaN}_3$  and (b)  $\text{NH}_4\text{Cl}$  contents on the product yield.

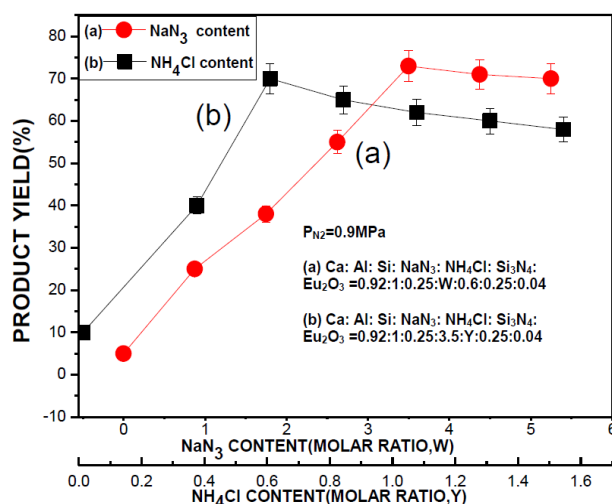
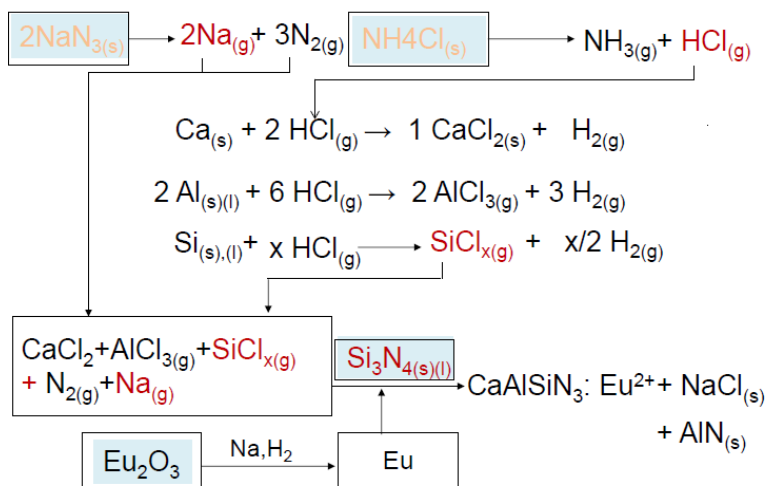


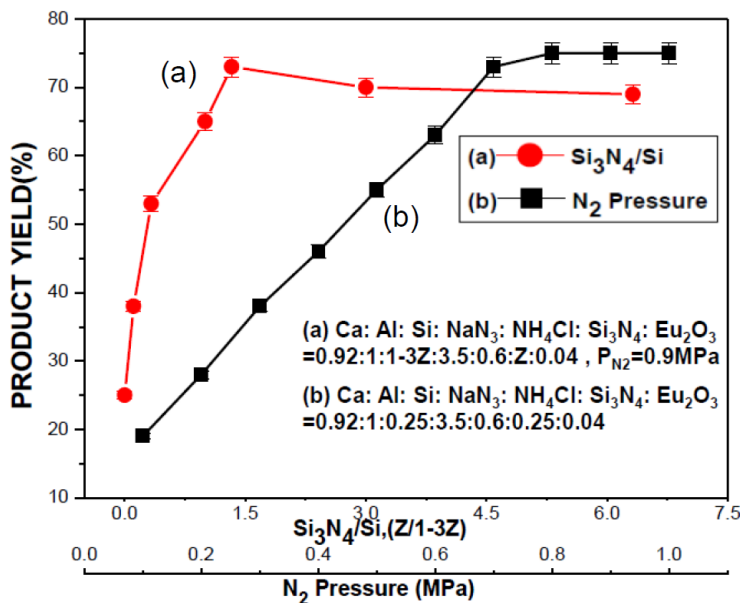
Figure 6. The proposed reaction mechanism.



2.2.2. Effects of  $\text{Si}_3\text{N}_4$

As mentioned previously, the product yield could be significantly increased by adding a proper amount of  $\text{Si}_3\text{N}_4$  to the reactant compact. In studying the effect of  $\text{Si}_3\text{N}_4$ , the total amount of Si (*i.e.*, the Si powder and the Si contained in the  $\text{Si}_3\text{N}_4$  powder) was kept constant at a molar ratio of 1 (being equal to that in the optimum synthesis condition) and the amount of  $\text{Si}_3\text{N}_4$  was expressed as the molar ratio of  $\text{Si}_3\text{N}_4$  to Si (*i.e.*,  $\text{Si}_3\text{N}_4/\text{Si}$ ). Curve (a) in Figure 7 shows the effects of  $\text{Si}_3\text{N}_4/\text{Si}$  on the product yield. As can be seen, the product yield increases with increasing  $\text{Si}_3\text{N}_4/\text{Si}$  to a maximum of  $\sim 74\%$  at  $\text{Si}_3\text{N}_4/\text{Si} = 1.33$  and begins to decrease with further increase in  $\text{Si}_3\text{N}_4/\text{Si}$ .

**Figure 7.** Effects of (a)  $\text{Si}_3\text{N}_4$  Content (expressed as the molar ratio of  $\text{Si}_3\text{N}_4/\text{Si}$ ) and (b)  $\text{N}_2$  pressure on the product yield.



When the reactant compact was prepared without addition of  $\text{Si}_3\text{N}_4$  (*i.e.*,  $\text{Si}_3\text{N}_4/\text{Si} = 0$ ), many large and spherical particles (with diameters up to 20  $\mu\text{m}$ ) were observed (with an SEM) on fractured surfaces of the as-synthesized products. These particles were identified by elementary analysis to be Si particles and they became smaller and were reduced in number when increasing  $\text{Si}_3\text{N}_4/\text{Si}$ . These spherical Si particles were believed to be formed by melting and coalescence of the Si particles added when preparing the reactant compact. Because formation of large and spherical particles decreases the surface area for solid (or liquid)-gas reactions, coalescence hinders the nitridation reaction, thus lowering the product yield. Coalescence of Si is believed to be reduced at the presence of  $\text{Si}_3\text{N}_4$  particles because the molten Si can spread over the  $\text{Si}_3\text{N}_4$  particles due to capillary force. This capillary spreading increases the surface area for solid (or liquid)-gas reaction. The product yield thus increases with increasing  $\text{Si}_3\text{N}_4/\text{Si}$  (in the range of  $\text{Si}_3\text{N}_4/\text{Si} < 1.33$ , see Figure 7). As the  $\text{Si}_3\text{N}_4/\text{Si}$  is further increased, the combustion temperature begins to decrease because of the cooling effect of a high content of  $\text{Si}_3\text{N}_4$  and also a less amount of Si available for combustion, thus resulting in a decrease in the product yield. As can be seen in Figure 3,  $\text{Si}_3\text{N}_4$  was not detected in the product by XRD. The  $\text{Si}_3\text{N}_4$  added to the reactant compact was thus believed to be converted completely to the product phase ( $\text{CaAlSiN}_3:\text{Eu}^{2+}$ ).

### 2.2.3. Effect of $\text{N}_2$ Pressure

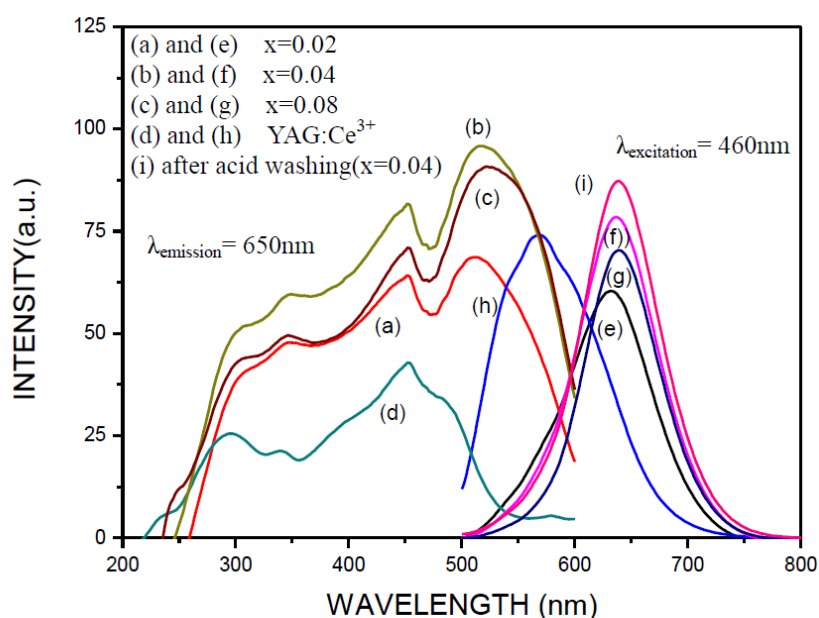
The effect of nitrogen pressure on the product yield is shown as curve (b) in Figure 7. (The reactant composition was kept the same as the optimum synthesis condition, *i.e.*, Ca:Al:Si: $\text{NaN}_3$ : $\text{NH}_4\text{Cl}$ : $\text{Si}_3\text{N}_4$ : $\text{Eu}_2\text{O}_3$  = 0.92:1:0.25:3.5:0.6:0.25:0.04). As can be seen, the product yield increases with increasing nitrogen pressure to  $\sim 75\%$  at nitrogen pressure of 0.9 MPa and becomes relatively unaffected at higher  $\text{N}_2$  pressures. The amount of nitrogen available to the combustion synthesis reaction increases with increasing nitrogen pressure. A higher  $\text{N}_2$  pressure thus results in a higher reaction rate, and thus a higher product yield (in the range of  $\leq 0.9$  MPa, see Figure 7). As a

sufficient amount of N<sub>2</sub> is supplied, the reaction rate and thus the product yield become relatively unaffected with further increase in the N<sub>2</sub> pressure (>0.9 MPa, see Figure 7).

### 2.3. Photoluminescence Properties of CaAlSiN<sub>3</sub>:Eu<sup>2+</sup> Phosphor

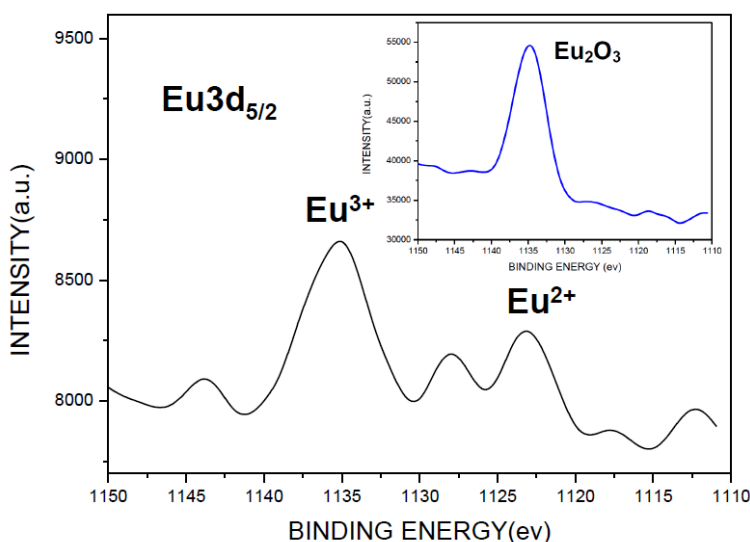
Curves (a), (b), and (c) and (e), (f), and (g) in Figure 8 are the excitation and emission spectra ( $\lambda_{\text{excitation}} = 460 \text{ nm}$ ), respectively, of the phosphor powders (after removing NaCl and the residual Si) synthesized under the optimum synthesis condition, that is Ca:Al:Si:NaN<sub>3</sub>:NH<sub>4</sub>Cl:Si<sub>3</sub>N<sub>4</sub>:Eu<sub>2</sub>O<sub>3</sub> = 0.92:1:0.25:3.5:0.6:0.25:*x* (*x* = 0.02, 0.04, and 0.08) and N<sub>2</sub> pressure = 0.9 MPa. As can be seen, the intensities of the excitation and emission both increase when the Eu<sub>2</sub>O<sub>3</sub> molar ratio (*x*) is increased from 0.02 to 0.04, but both decrease when the Eu<sub>2</sub>O<sub>3</sub> molar ratio is further increased to 0.08. The excitation spectra all consist of two main absorption bands: The one in the range of 200–350 nm is ascribed to the host lattice excitation due to transition from the valence to the conduction band. The other excitation band being in the range of 350–600 nm is assigned to the 4f<sup>7</sup> → 4f<sup>6</sup>5d<sup>1</sup> transition of the Eu<sup>2+</sup> ion. All the emission spectra show a single broad band emission in the range of 500–800 nm (which are similar to the literature) and are attributed to the allowed 4f<sup>6</sup>5d<sup>1</sup> → 4f<sup>7</sup> transition of the Eu<sup>2+</sup> ion. For comparison, similar spectra of a commercially available YAG:Ce<sup>3+</sup> phosphor (P46-Y3) were also measured (under the same measurement conditions as those for the synthesized phosphors) and are shown as curves (d) and (h) in Figure 8. As can be seen, the peak emission intensity of the synthesized phosphor is ~106% of that of YAG:Ce<sup>3+</sup> at 0.04 of the Eu<sub>2</sub>O<sub>3</sub> molar ratio. Internal quantum efficiencies (IQE) of the synthesized phosphor and the commercial YAG:Ce<sup>3+</sup> (P46-Y3) phosphor were also measured (with  $\lambda_{\text{excitation}} = 460 \text{ nm}$ ) to be 71% and 69%, respectively. By comparison, the emission wavelength range measured in the present study is similar to those reported in many other studies [22–25] and the emission intensity is comparable to that reported by Piao *et al.* [26] for a similar phosphor.

**Figure 8.** The excitation ((a), (b) and (c)) and emission ((e), (f), (g) and (i)) spectra of the phosphor synthesized in this study and similar spectra of YAG: Ce<sup>3+</sup> phosphor (P46-Y3) are also shown ((d) and (h)) for comparison.



As can be seen in Figure 8, the emission intensity depends strongly on the  $\text{Eu}_2\text{O}_3$  content in the reactant compact. A question thus arises that whether or not the added  $\text{Eu}_2\text{O}_3$  is completely incorporated into the host lattice. To clarify this problem, XPS was employed to identify the chemical state of the Eu. As shown in Figure 9, in addition to the characteristic peak of  $\text{Eu}^{2+}$  (at 1123 eV [27–30]), the characteristic peak of  $\text{Eu}^{3+}$  (at 1135 eV [27–30]) was also detected for the synthesized product, which is located at the same position as that of the  $\text{Eu}_2\text{O}_3$  added to the reactant (the inset in Figure 9). Since sharp line emission peaks, characteristic of  $^5\text{D}_0 \rightarrow ^7\text{F}_J$  transition of  $\text{Eu}^{3+}$  [31], were not observed (see Figure 8),  $\text{Eu}^{3+}$  is not considered to be incorporated into the host lattice. These results thus indicate that a certain fraction of  $\text{Eu}_2\text{O}_3$  was unreacted and contained in the product. Therefore, the actual concentration of  $\text{Eu}^{2+}$  in the host lattice is believed to be lower than that calculated based on the reactant composition. The unreacted  $\text{Eu}_2\text{O}_3$  contained in the product can be removed by washing the product with hydrochloric acid. As shown in Figure 8 (curve (i)), the emission intensity of the synthesized phosphor increases slightly after this acid washing.

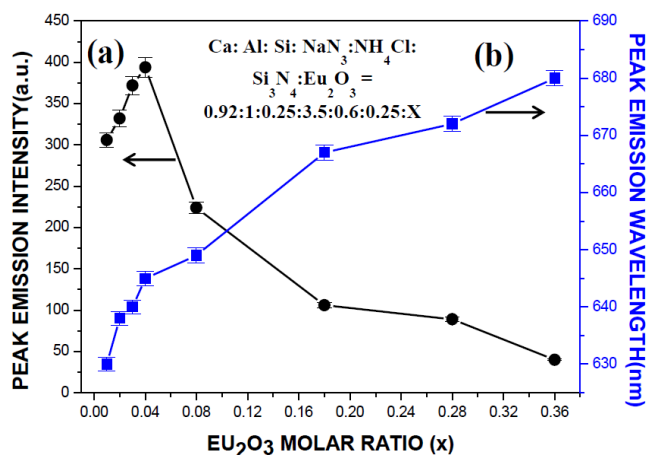
**Figure 9.** XPS spectra in the Eu  $3d_{5/2}$  region of reactant  $\text{Eu}_2\text{O}_3$  (inset) and the synthesized product.



The dependence of the peak emission intensity and wavelength on the  $\text{Eu}_2\text{O}_3$  molar ratio (*i.e.*, the  $x$  in  $\text{Ca:Al:Si:NaN}_3:\text{NH}_4\text{Cl:Si}_3\text{N}_4:\text{Eu}_2\text{O}_3 = 0.92:1:0.25:3.5:0.6:0.25:x$ ) is shown in Figure 10. The peak emission intensity increases with increasing  $\text{Eu}_2\text{O}_3$  molar ratio to a maximum at the molar ratio of 0.04 and begins to decrease with further increase in the molar ratio. At the same time, the emission band shows a redshift: The peak emission wavelength increases from 630 to 680 nm as the  $\text{Eu}_2\text{O}_3$  molar ratio is increased from 0.01 to 0.18. Although a certain fraction of  $\text{Eu}_2\text{O}_3$  was found unreacted, the  $\text{Eu}^{2+}$  concentration in the lattice of the product phase increases with increasing  $\text{Eu}_2\text{O}_3$  molar ratio in the range of this study. This is seen in Figure 10 where the peak emission wavelength increases continuously with increasing  $\text{Eu}_2\text{O}_3$  molar ratio. The decrease in peak emission intensity beyond a critical  $\text{Eu}^{2+}$  concentration (where the  $\text{Eu}_2\text{O}_3$  molar ratio is 0.04, see Figure 10) is considered to be due to concentration quenching, which occurred when the interatomic distance among the  $\text{Eu}^{2+}$  ions is shortened, causing frequent energy transfer among them [32]. The redshift can be due to an increase in probability of the energy transfer of  $\text{Eu}^{2+}$  from higher to lower levels of  $5d$ , thus increasing the emission intensity in the

long wavelength region [33]. As pointed out in many other studies [34–36], the redshift may also be explained by reabsorption due to overlapping of the excitation and the emission spectra. Note that the overlapping of the excitation and the emission spectra is seen in Figure 8 to increase with increasing  $\text{Eu}_2\text{O}_3$  molar ratio. In addition, the incorporation of  $\text{Eu}^{2+}$  on  $\text{Ca}^{2+}$  site results in distortion of the lattice, which may also contribute to the redshift of the emission [37].

**Figure 10.** Dependence of (a) peak emission intensity and (b) peak emission wavelength on the  $\text{Eu}_2\text{O}_3$  molar ratio,  $x$ .



### 3. Experimental Section

#### 3.1. Development of the Process

As mentioned previously, this study is aimed at developing a combustion synthesis process for synthesis of  $\text{CaAlSiN}_3\text{:Eu}^{2+}$  phosphor at low  $\text{N}_2$  pressures by using reactants which can be handled in ambient air. Based on this thought, Ca, Al, Si and  $\text{Eu}_2\text{O}_3$  powders were chosen as the reactants serving as the sources of Ca, Al, Si, and Eu in  $\text{CaAlSiN}_3\text{:Eu}^{2+}$  phosphor. However, it was found that the compact of the mixture of these powders (referred to as reactant compact hereafter) could not be ignited under a  $\text{N}_2$  pressure limited to the reactor used in the present study (*i.e.*,  $\leq 1.0$  MPa). This was considered to be due to the low reactivity of Ca, Si with respect to  $\text{N}_2$  at pressures of  $\leq 1.0$  MPa. The reactant compact was thus wrapped up with an igniting agent (*i.e.*, the mixture of Mg and  $\text{Fe}_3\text{O}_4$  powders), which can undergo a high exothermic combustion reaction, thus heating up quickly the reactant compact and causing its combustion reaction to occur. Besides, it was found that the product yield could be significantly enhanced by adding proper amounts of  $\text{NaN}_3$ ,  $\text{NH}_4\text{Cl}$  and  $\text{Si}_3\text{N}_4$  simultaneously. In the combustion synthesis process developed in the present study, the reactant compact is thus composed of Ca, Al, Si,  $\text{Eu}_2\text{O}_3$ ,  $\text{NaN}_3$ ,  $\text{NH}_4\text{Cl}$  and  $\text{Si}_3\text{N}_4$  and the reactant compact is wrapped up with an igniting agent.

#### 3.2. Description of Experiment

Listed in Table 1 are the characteristics of the reagents used in this study. Silicon, aluminum, calcium, europium oxide, sodium azide, ammonium chloride and silicon nitride powders were thoroughly mixed in the desired proportions and then pressed into cylindrical compacts (*i.e.*, the reactant compacts) with

17 mm in diameter and ~16 mm in length. A stainless steel die with two plungers was used and a pressure of 300 MPa was uniaxially applied in forming the compacts. The reactant compact thus obtained was placed in a larger die and the space between the compact and the die was filled with an igniting agent (*i.e.*, a mixed powder of Mg and Fe<sub>3</sub>O<sub>4</sub> at 4:1 molar ratio). By uniaxially applying a pressure of 300 MPa, the reactant compact was wrapped up with the igniting agent, which was a larger cylindrical compact (referred to as a wrapped compact, see the insert in Figure 1) with 30 mm in diameter and ~30 mm in length.

**Table 1.** Characteristics of the reagents used in this study.

Reagent	Particle Size (um)	Purity (%)	Source
Si	1–5	99	Alfa Aesar
Ca	<963	99.5	Alfa Aesar
Eu <sub>2</sub> O <sub>3</sub>	2.5–6	99.99	Seedchem Company
NaN <sub>3</sub>	$d_{50} \cong 150$	99	Johnson Matthey
NH <sub>4</sub> Cl	–	99	Panreac
Al	$d_{50} \cong 3$	99	First Chemical Work
$\alpha$ -Si <sub>3</sub> N <sub>4</sub>	$d_{50} \cong 10$	95	Alfa Aesar
Mg	$d_{50} \cong 20$	99	Nihon Shiyaku
Fe <sub>3</sub> O <sub>4</sub>	$d_{50} \cong 102$	99	Nihon Shiyaku
N <sub>2</sub>	Gas	99	Yun Shan

The combustion synthesis reactor used in this study has been described and shown schematically in our previous studies [38–42] and thus is not repeated here. The wrapped compact was placed on a height adjustable stage which was adapted so that the top surface of the compact was about 5 mm below the tungsten heating coil. The reactor was evacuated to 65 Pa by flushing with nitrogen between the evacuations. After the evacuation, the reactor was backfilled with nitrogen to the desired pressures. The combustion reaction was ignited by heating the top surface of the compact for ~10 s by applying an electrical power of ~1 KW to the heating coil.

Variation of temperature during combustion reaction was measured by using 0.13 mm diameter W-5%Re-W-26%Re thermocouples. The thermocouples, insulated with 1.2 mm diameter alumina tubes, were inserted into the compact at appropriate depths by first drilling holes. As shown by the insert in Figure 1, the temperature variation of the reactant compact was measured by thermocouple A while that of the igniting agent was measured by thermocouple B. After combustion, the igniting agent was converted to MgO+Fe, which was loosely attached to the interior product. The interior product could thus be easily separated from the combustion product of the igniting agent. The as-synthesized products contained byproducts, AlN and NaCl, and small amounts of unreacted Si. NaCl could be removed by washing the products with water and unreacted Si could be removed by washing the products with an acid (*e.g.*, a mixed solution of 48 wt% HF<sub>(aq)</sub> and 68 wt% HNO<sub>3(aq)</sub> at a volume ratio of 5:1 as used in this study). The product yield (defined as the percentage of the Si converted to the product) was obtained from the weight ratio of the Si contained in the product (being assumed to be all CaAlSiN<sub>3</sub>:Eu<sup>2+</sup> after removal of NaCl and unreacted Si) to that in the reactant compact (including the Si powder and the Si in Si<sub>3</sub>N<sub>4</sub>). The crystalline phase of the product was identified by X-ray diffraction (XRD, DMAX-200/PC, Rigaku, Tokyo, Japan) using Cu K $\alpha$  radiation operating at 40kV and 30 mA. The data was collected at a scanning

speed of 10°/min between 20° and 80° with a scanning step of 0.01° in 2 $\theta$ . The morphology of the product was analyzed with a scanning electron microscope (S-4100, Hitachi, Tokyo, Japan). The particle size distribution was measured by a particle size analyzer (LA-950, Horiba, Tokyo, Japan). The excitation and emission spectra were measured at room temperature using a fluorescent spectrophotometer (FP-6600, Jasco, Tokyo, Japan) with a 150 W xenon lamp at a scanning speed of 125 nm/min. The internal quantum efficiency [43] was measured using a fluorescent spectrometer (F-7000; Hitachi, Tokyo, Japan) with an integrating sphere system (5JO-0148; Hitachi, Tokyo, Japan). The light from a 200 W xenon lamp was used as the excitation source at a scanning speed of 240 nm/min. The chemical states of elements were measured by X-ray photoelectron spectroscopy with an Al K $\alpha$  X-ray source (ESCA-LAB 250, VG Scientific, London, UK).

#### 4. Conclusions

A combustion synthesis method has been developed for synthesis of CaAlSiN<sub>3</sub>:Eu<sup>2+</sup> phosphor at low N<sub>2</sub> pressures by using reactants which can be handled in ambient air. The synthesis reaction is triggered by the combustion of an igniting agent, which is ignited by heating for ~10 s with an electrical power of ~1 KW and it takes ~10 s for the synthesis reaction to complete. In addition to easy handling of the reactants and a low N<sub>2</sub> pressure required (~0.9 MPa), the method developed in the present study possesses many other advantages including simple and inexpensive equipment required, relatively low cost of the reactants, a fast reaction and short processing time, potential capability for mass production and possibly low production costs. The synthesized CaAlSiN<sub>3</sub>:Eu<sup>2+</sup> phosphor absorbs light in the region of 200–600 nm and shows a broad band emission in the region of 500–800 nm. The sample doped with Eu<sup>2+</sup> at the optimized molar ratio of 0.04 is efficiently excited by the blue light (460 nm) and generates emission peaking at ~650 nm with peak emission intensity exceeding that of the YAG:Ce<sup>3+</sup> (P46-Y3) phosphor by ~6%. The internal quantum efficiency of the synthesized phosphor was measured to be 71%, compared to 69% of the YAG:Ce<sup>3+</sup> (P46-Y3). With further improvement, the combustion synthesis method developed in the present study may be potentially applied for industrial production of phosphors for application in white LED lighting.

#### Acknowledgments

Support of this research by the National Science Council of the Republic of China under Grant No. NSC 102-2221-E-006-222 is gratefully acknowledged.

#### Author Contributions

The process design, experimental work and writing of the first draft of the manuscript were all carried out and finished by Shu-Chi Huang. The following correction, modification and revision of the manuscript were also performed by Shu-Chi Huang under the supervision of Shyan-Lung Chung.

#### Conflicts of Interest

The authors declare no conflict of interest.

## References

1. Smet, P.F.; Parmentier, A.B.; Poelman, D. Selecting conversion phosphors for white light-emitting diodes. *J. Electrochem. Soc.* **2011**, *158*, R37–R54.
2. Nakamura, S.; Mukai, T.; Senoh, M. Candela-class high-brightness InGaN/AlGaN double heterostructure blue-light-emitting diodes. *Appl. Phys. Lett.* **1994**, *64*, 1687–1689.
3. Rohwer, L.S.; Srivastava, A.M. Development of Phosphors for LEDs. *Electrochem. Soc. Interface* **2003**, 36–39.
4. Taso, J.Y. *Light Emitting Diodes (LEDs) for General Illumination Update*; Optoelectronics Industry Development Association: Washington, DC, USA, 2002.
5. Chung, S.L.; Huang, S.C.; Chou, W.C.; Tangguh, W. Phosphors based on nitridosilicates: Synthesis methods and luminescent properties. *Curr. Opin. Chem. Eng.* **2014**, *3*, 62–67.
6. Li, Y.Q.; van Steen, J.E.J.; van Kreveld, J.W.H.; Botty, G.; Delsing, A.C.A.; DiSalvo, F.J.; de With, G.; Hintzen, H.T. Luminescence properties of red-emitting  $M_2Si_5N_8:Eu^{2+}$  (M = Ca, Sr, Ba) LED conversion phosphors. *J. Alloy. Compd.* **2006**, *417*, 273–279.
7. Piao, X.; Horikawa, T.; Hanzawa, H.; Machida, K.I. Photoluminescence properties of  $Ca_2Si_5N_8:Eu^{2+}$  nitride phosphor prepared by carbothermal reduction and nitridation method. *Chem. Lett.* **2006**, *35*, 334–335.
8. Watanabe, H.; Yamane, H.; Kijima, N. Crystal structure and luminescence of  $Sr_{0.99}Eu_{0.01}AlSiN_3$ . *J. Solid State Chem.* **2008**, *181*, 1848–1852.
9. Hoppe, H.A.; Lutz, H.; Morys, P.; Schnick, W.; Seilmeier, A. Luminescence in  $Eu^{2+}$ -doped  $Ba_2Si_5N_8$  fluorescence, thermoluminescence, and upconversion. *J. Phys. Chem. Solids* **2000**, *61*, 2001–2006.
10. Li, H.L.; Xie, R.J.; Hirosaki, N.; Takeda, T.; Zhou, G.H. Synthesis and luminescence properties of orange-red-emitting  $M_2Si_5N_8:Eu^{2+}$  (M = Ca, Sr, Ba) light-emitting diode conversion phosphors by a simple nitridation of  $MSi_2$ . *Int. J. Appl. Ceram. Technol.* **2009**, *6*, 459–464.
11. Zeuner, M.; Hintze, F.; Schnick, W. Low temperature precursor route for highly efficient spherically shaped LED-phosphors  $M_2Si_5N_8:Eu^{2+}$  (M = Eu, Sr, Ba). *Chem. Mater.* **2008**, *21*, 336–342.
12. Kim, Y.S.; Choi, S.W.; Park, J.H.; Bok, E.; Kim, B.K.; Hong, S.H. Redemitting (Sr,Ca)AlSiN<sub>3</sub>:Eu<sup>2+</sup> phosphors synthesized by spark plasma sintering. *ECS J. Solid State Sci. Technol.* **2013**, *2*, R3021–R3025.
13. Yang, J.J.; Wang, T.; Chen, D.C.; Chen, G.D.; Liu, Q.L. An investigation of  $Eu^{2+}$ -doped  $CaAlSiN_3$  fabricated by an alloy-nitridation method. *Mater. Sci. Eng. B* **2012**, *177*, 1596–1604.
14. Chen, C.C.; Chen, W.J.; Rainwater, B.; Liu, L.; Zhang, H.; Liu, Y.; Guo, X.; Zhou, J.; Xie, E.  $M_2Si_5N_8:Eu^{2+}$ -based (M = Ca, Sr) red-emitting phosphors fabricated by nitrate reduction process. *Opt. Mater.* **2011**, *33*, 1585–1590.
15. Merzhanov, A.G.; Borovinskaya, I.P. A new class of combustion processes. *Combust. Sci. Technol.* **1975**, *10*, 195–201.
16. Chung, S.L.; Chou, W.C. Combustion synthesis of  $Ca_2Si_5N_8:Eu^{2+}$  phosphors and their luminescent properties. *J. Am. Ceram. Soc.* **2013**, *96*, 2086–2092.
17. Hu, Y.S.; Zhuang, W.D.; He, H.Q.; Liu, R.H.; Chen, G.T.; Liu, Y.H.; Huang, X.W. High temperature stability of  $Eu^{2+}$ -activated nitride red phosphors. *J. Rare Earth* **2014**, *32*, 12–16.

18. Li, J.; Watanabe, T.; Wada, H.; Setoyama, T.; Yoshimura, M. Low-temperature crystallization of Eu-doped red-emitting  $\text{CaAlSiN}_3$  from alloy-derived ammonometallates. *Chem. Mater.* **2007**, *19*, 3592–3594.
19. Xie, R.J.; Hirotsuki, N.; Sakuma, K.; Kimura, N. White light-emitting diodes (LEDs) using (oxy)nitride phosphors. *J. Phys. D Appl. Phys.* **2008**, *41*, doi:10.1088/0022-3727/41/14/144013.
20. Kubus, M.; Meyer, H.J.; Anorg, Z. A Low-temperature synthesis route for  $\text{CaAlSiN}_3$  doped with  $\text{Eu}^{2+}$ . *Allg. Chem.* **2013**, *639*, 669–672.
21. Chung, S.L.; Chang, C.W.; Cadete Santos Aires, F.J. Reaction mechanism in combustion synthesis of  $\alpha\text{-Si}_3\text{N}_4$  powder using  $\text{NaN}_3$ . *J. Mater. Res.* **2008**, *23*, 2720–2726.
22. Lin, C.C.; Zheng, Y.S.; Chen, H.Y.; Ruan, C.H.; Xiao, G.W.; Liu, R.S. Improving optical properties of white LED fabricated. *J. Electrochem. Soc.* **2010**, *157*, H900–H903.
23. Hu, W.W.; Cai, C.; Zhu, Q.Q.; Xu, X.; Hao, L.Y.; Agathopoulos, S. Preparation of high performance  $\text{CaAlSiN}_3\text{:Eu}^{2+}$  phosphors with the aid of  $\text{BaF}_2$  flux. *J. Alloy. Comp.* **2014**, *613*, 226–231.
24. Cai, C.; Qian, J.; Zhang, B.; Hu, W.; Hao, L.; Xu, X.; Wang, Y. Synthesis of red-emitting  $\text{CaAlSiN}_3\text{:Eu}^{2+}$  phosphors through a cost-effective synthetic route. *ECS J. Solid State Sci. Technol.* **2014**, *3*, R169–R172.
25. Lei, B.; Machida, K.I.; Horikawa, T.; Hanzawa, H. Synthesis and photoluminescence properties of  $\text{CaAlSiN}_3\text{:Eu}^{2+}$  nanocrystals. *Chem. Lett.* **2010**, *39*, 104–105.
26. Piao, X.; Machida, K.I.; Horikawa, T.H.; Hanzawa, Y.; Shimomura, Y.; Kijima, N. Preparation of  $\text{CaAlSiN}_3\text{:Eu}^{2+}$  phosphors by the self-propagating high-temperature synthesis and their luminescent properties. *Chem. Mater.* **2007**, *19*, 4592–4599.
27. Mercier, F.; Alliot, C.; Bion, L.; Thromat, N.; Toulhoat, P. XPS study of Eu(III) coordination compounds: Core levels binding energies in solid mixed-oxo-compounds  $\text{Eu}_m\text{X}_x\text{O}_y$ . *J. Electron. Spectrosc.* **2006**, *150*, 21–26.
28. Lacanilao, A.; Wallez, G.; Mazerolles, L.; Dubot, P.; Binet, L.; Pavageau, B.; Servant, L.; Buissette, V.; Mercier, T.L. Structural analysis of thermal degradation and regeneration in blue phosphor  $\text{BaMgAl}_{10}\text{O}_{17}\text{:Eu}^{2+}$  based upon cation diffusion. *Solid. State Ionics* **2013**, *253*, 32–38.
29. Kang, J.G.; Jung, Y.; Min, B.K.; Sohn, Y. Full characterization of  $\text{Eu}(\text{OH})_3$  and  $\text{Eu}_2\text{O}_3$  nanorods. *Appl. Surf. Sci.* **2014**, *314*, 158–165.
30. Kumar, V.; Kumar, V.; Som, S.; Duvenhage, M.M.; Ntwaeaborwa, O.M.; Swart, H.C. Effect of Eu doping on the photoluminescence properties of ZnO nanophosphors for red emission applications. *Appl. Surf. Sci.* **2014**, *308*, 419–430.
31. Wang, Z.; Guo, S.; Li, Q.; Zhang, X.; Li, T.; Li, P.; Yang, Z.; Guo, Q. Luminescent properties of  $\text{Ba}_2\text{SiO}_4\text{:Eu}^{3+}$  for white light emitting diodes. *Phys. B. Condens. Matter* **2013**, *411*, 110–113.
32. Dexter, D.L. A theory of sensitized luminescence in solids. *J. Chem. Phys.* **1953**, *21*, 836–850.
33. Blasse, G. Energy transfer between inequivalent  $\text{Eu}^{2+}$  ions. *J. Solid State Chem.* **1986**, *62*, 207–211.
34. Li, Y.Q.; Delsing, A.C.; de With, A.G.; Hintzen, H.T. Luminescence properties of  $\text{Eu}^{2+}$ -activated alkaline-earth silicon-oxynitride  $\text{MSi}_2\text{O}_{2-\delta}\text{N}_{2+2/3\delta}$  ( $M = \text{Ca}, \text{Sr}, \text{Ba}$ ): A promising class of novel LED conversion phosphors. *Chem. Mater.* **2005**, *17*, 3242–3248.
35. Avci, N.; Korthout, K.; Newton, M.A.; Smet, P.F.; Poelman, D. Valence states of europium in  $\text{CaAl}_2\text{O}_4\text{:Eu}$  phosphors. *Opt. Mater. Exp.* **2012**, *2*, 321–330.

36. Jang, B.Y.; Park, J.S. Luminescence properties of Eu<sub>2</sub>O<sub>3</sub>-doped Ca<sub>2</sub>Si<sub>5</sub>N<sub>8</sub> phosphors. *J. Ceram. Process. Res.* **2009**, *10*, 844–847.
37. Xie, R.J.; Hirosaki, N.; Suehiro, T.; Xu, F.F.; Mamoru, M. A simple, efficient synthetic route to Sr<sub>2</sub>Si<sub>5</sub>N<sub>8</sub>:Eu<sup>2+</sup>-based red phosphors for white light-emitting diodes. *Chem. Mater.* **2006**, *18*, 5578–5583.
38. Lee, W.C.; Tu, C.L.; Weng, C.U.; Chung, S.L. A novel process for combustion synthesis of AlN powder. *J. Mater. Res.* **1995**, *10*, 774–778.
39. Chung, S.L.; Yu, W.L.; Lin, C.N. A self-propagating high temperature synthesis method for synthesis of AlN powder. *J. Mater. Res.* **1999**, *14*, 1928–1933.
40. Lin, C.N.; Chung, S.L. Combustion synthesis of aluminum nitride powder using additives. *J. Mater. Res.* **2001**, *16*, 2200–2208.
41. Lin, C.N.; Chung, S.L. Combustion synthesis method for synthesis of aluminum nitride powder using aluminum containers. *J. Mater. Res.* **2001**, *16*, 3518–3525.
42. Lin, C.N.; Chung, S.L. Combustion synthesis method for synthesis of aluminum nitride powder using aluminum containers (II). *J. Mater. Res.* **2004**, *19*, 3037–3045.
43. Moreno, L.A. Absolute quantum yield measurement of powder samples. *J. Vis. Exp.* **2012**, *63*, doi:10.3791/3066.

© 2014 by the authors; licensee MDPI, Basel, Switzerland. This article is an open access article distributed under the terms and conditions of the Creative Commons Attribution license (<http://creativecommons.org/licenses/by/4.0/>).